DISCLAIMER

This report was prepared as an account of work sponsored by an agency of the United States Government. Neither the United States Government nor any agency thereof, nor any of their employees, makes any warranty, express or implied, or assumes any legal liability or responsibility for the accuracy, completeness, or usefulness of any information, apparatus, product, or process disclosed, or represents that its use would not infringe privately owned rights. Reference herein to any specific commercial product, process, or service by trade name, trademark, manufacturer, or otherwise does not necessarily constitute or imply its endorsement, recommendation, or favoring by the United States Government or any agency thereof. The views and opinions of authors expressed herein do not necessarily state or reflect those of the United States Government or any agency thereof. Reference herein to any social initiative (including but not limited to Diversity, Equity, and Inclusion (DEI); Community Benefits Plans (CBP); Justice 40; etc.) is made by the Author independent of any current requirement by the United States Government and does not constitute or imply endorsement, recommendation, or support by the United States Government or any agency thereof.

Euler equations and the Sod shock tube problem

Justin Angus[1] and Joshua Ludwig[1]

[1]Lawrence Livermore National Laboratory

January 2025

1 Introduction

The Euler equations are a subset of the magnetohydrodynamic (MHD) equations in the infinitely collisional, unmagnetized limit. MHD modeling is central to many areas of plasma physics, ranging from low-temperature glow discharges to inertial confinement fusion. An important aspect of the Euler equations is their ability to describe states with discontinuities, such as shock waves. A standard benchmark test for numerical implementation of the Euler equations is the Sod shock tube [6]. In this test, the system is initialized at rest with a pressure and density discontinuity, which results in a shock wave traveling into the low-pressure region and a rarefaction wave traveling into the high-pressure region. Starting with the presentation of the Euler equations, a numerical algorithm is presented here to solve these equations in one dimension. This is followed by an overview of the Sod shock tube problem that includes the precise initial setup and the analytic solution. Finally, the analytic solution is compared with results from numerical simulations.

2 Governing Equations

In the inviscid, unmagnetized limits, the ideal MHD equations reduce to the well-known Euler equations, which are conservation laws for mass, momentum, and energy and are a prototypical example of a hyperbolic system. In one-dimension, the Euler equations can be written as

$$\frac{\partial \mathbf{w}}{\partial t} + \frac{\partial \mathbf{F}(\mathbf{w})}{\partial x} = 0, \tag{1}$$

where the solution vector $\mathbf{w}$ and the flux $\mathbf{F}(\mathbf{w})$ are defined, respectively, as

$$\mathbf{w} = \begin{bmatrix} \rho \\ \rho u \\ \mathcal{E} \end{bmatrix}, \quad \text{and} \quad \mathbf{F}(\mathbf{w}) = \begin{bmatrix} \rho u \\ \rho u^2 + P \\ (\mathcal{E} + P)\, u \end{bmatrix}. \tag{2}$$

Here, ρ is the mass density, u is the fluid velocity, and $\mathcal{E} = \rho u^2/2 + P/(\gamma - 1)$ is the energy density with P the fluid pressure and γ the adiabatic coefficient. For an ideal atomic gas, $\gamma = 5/3$. For

an ideal diatomic gas, which has additional degrees of freedom associated with vibrational and rotational states, $\gamma = 7/5 = 1.4$.

The eigenvalues of the flux Jacobian $\partial\mathbf{F}/\partial\mathbf{w}$ are $\lambda = [u \pm C_s, u]$, where $C_s \equiv \sqrt{\gamma P/\rho}$ is the adiabatic sound speed. These eigenvalues, along with their corresponding eigenvectors, are fundamental to understanding solutions of the Euler equations in terms of Riemann invariants associated with characteristic families. In layman's terms, there exist certain scalar quantities that are constant along trajectories governed by $dx/dt = \lambda$.

3 Numerical algorithm

The numerical algorithm used to solve Eqs. 1-2 is described in this subsection. The equations are discretized with uniform spacing on a 1D grid (see Fig. 1). The flux divergence operator is computed using a second-order finite-volume method. The discrete state vector lives at cell centers: $\mathbf{w}_{i+1/2} = \left[\rho_{i+1/2}, m_{i+1/2}, \mathcal{E}_{i+1/2}\right]$. The discrete fluxes are computed at cell interfaces. Starting with the state variables at some time t_n, the second-order predictor-correct method used to advance the variables to time t_{n+1} is

$$\text{Stage 1}: \quad \mathbf{w}_{i+1/2}^{n+1/2} = \mathbf{w}_{i+1/2}^{n} - \frac{\Delta t}{2}\frac{\mathbf{F}_{i+1}^{n} - \mathbf{F}_{i}^{n}}{\Delta x}, \tag{3}$$

$$\text{Stage 2}: \quad \mathbf{w}_{i+1/2}^{n+1} = \mathbf{w}_{i+1/2}^{n} - \Delta t\frac{\mathbf{F}_{i+1}^{n+1/2} - \mathbf{F}_{i}^{n+1/2}}{\Delta x}. \tag{4}$$

Here, $\Delta x = x_{i+1} - x_i$ is the uniform grid spacing and Δt is the time step, which doesn't necessarily have to be uniform from step to step but is uniform for each stage of a given step. The finite-volume method is preferred over finite-difference methods for hyperbolic conservation laws because it conserves discrete definitions of the conserved variables to machine precision. This is because whatever fluxes out of one cell in a time step is equal to that fluxed into the neighboring cell.

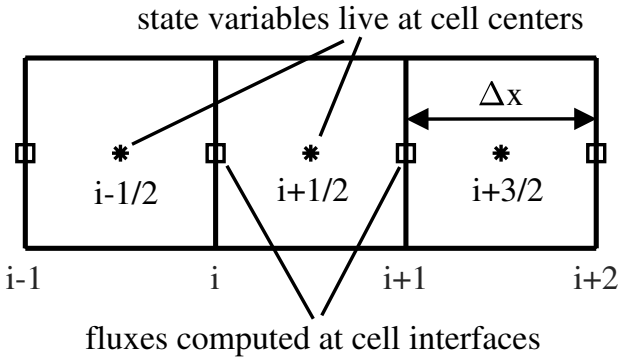

Figure 1: One dimensional finite volume grid.

The most complicated part of the algorithm is how to compute the fluxes at the cell interface. The simplest approach is to compute the fluxes point-wise at cell center using the cell-centered state variables and then interpolate these fluxes to cell interfaces using a second-order centered

interpolation. However, such an approach is known to result in spurious non-monotonic behavior of the variables for a simple 1D convection problem. The solution to the 1D convection problem is to use an upwind scheme where the flux at cell interfaces is computed using state variables upstream of the direction of the flow. Upwind methods also work for the Euler equations, but one must properly respect the characteristics of the nonlinear flux when formulating the stencil.

Here, we use the Lax-Friedrich flux-splitting approach [8, 5]. The first step in this method is to write the state vector as $\mathbf{w} = (\mathbf{w}_R + \mathbf{w}_L)/2$, where

$$\mathbf{w}_{R,L} = \mathbf{w} \pm \frac{\mathbf{F}}{\lambda_{\max}}, \tag{5}$$

and $\lambda_{\max} = |u| + C_s$ is the maximum eigenvalue of the flux Jacobian, which is also referred to as the flux-freezing speed. Similarly, the hyperbolic conservation law is replaced with the following set of advection equations:

$$\frac{\partial \mathbf{w}_R}{\partial t} + \frac{\partial \mathbf{F}_R}{\partial x} = 0, \text{ with } \mathbf{F}_R = \lambda_{\max}\mathbf{w}_R = \mathbf{F} + \lambda_{\max}\mathbf{w}, \tag{6}$$

$$\frac{\partial \mathbf{w}_L}{\partial t} + \frac{\partial \mathbf{F}_L}{\partial x} = 0, \text{ with } \mathbf{F}_L = -\lambda_{\max}\mathbf{w}_L = \mathbf{F} - \lambda_{\max}\mathbf{w}. \tag{7}$$

What this method essentially does is to decompose the state into left and right moving waves, for which it is then straight-forward to solve numerically using standard upwinding schemes. One difference between this scheme and the more sophisticated Godunov or Roe methods is that all characteristics are upwinded using the maximum eigenvalue, which adds extra numerical diffusion into the system. However, this scheme has advantages in that it is simpler to implement and it also avoids entropy-violating solutions [5]. The discrete versions of Eqs. 6-7 are identical to the form given in Eqs. 3-4. Numerical stability of this explicit scheme demands that $\Delta t < \Delta x/\lambda_{\max}$.

The analysis above where the state variable and fluxes are split is just a formality to understand how to properly compute the fluxes. In practice, the discrete stencil for $\mathbf{w}$ is exactly as given in Eqs. 3-4 with the flux at cell interfaces computed as

$$\mathbf{F}_i = \frac{\mathbf{F}_{R,i} + \mathbf{F}_{L,i}}{2}. \tag{8}$$

Using first-order upwinding, the left and right-going fluxes at the cell interfaces are $\mathbf{F}_{R,i} = \mathbf{F}_{R,i-1/2}$ and $\mathbf{F}_{L,i} = \mathbf{F}_{L,i+1/2}$, and the total flux can be written explicitly in terms of cell-centered quantities as

$$\mathbf{F}_i = \frac{\mathbf{F}_{i-1/2} + \lambda_{\max,i-1/2}\mathbf{w}_{i-1/2} + \mathbf{F}_{i+1/2} - \lambda_{\max,i+1/2}\mathbf{w}_{i+1/2}}{2}. \tag{9}$$

First order upwinding is stable, but it is too diffusive. A flux limiter is introduced in the following subsection that can be used to make the flux second order accurate away from regions of sharp gradients, such as shocks. The scheme will still be first-order accurate in the vicinity of shocks, which is a requirement for ensuring monotonic behavior of the solution [7].

3.1 Flux limiter

The analysis here closely follows that in Sec. 4.1 *Total Variation Diminishing (TVD) Schemes* in Ref. [7]. The right and left going fluxes in Eq. 8 can be written as

$$\mathbf{F}_{R,i} = \mathbf{F}^{(0)}_{R,i} + \Delta\mathbf{F}_{R,i}, \text{ and } \mathbf{F}_{L,i} = \mathbf{F}^{(0)}_{L,i} + \Delta\mathbf{F}_{L,i}, \tag{10}$$

where $\mathbf{F}^{(0)}_{R,i} = \mathbf{F}_{R,i-1/2}$ and $\mathbf{F}^{(0)}_{L,i} = \mathbf{F}_{L,i+1/2}$ are the first-order upwind fluxes and $\Delta\mathbf{F}_{R,i}$ and $\Delta\mathbf{F}_{L,i}$ are yet-to-be-defined corrections. We define two second-order flux corrections for right-moving waves:

$$\Delta\mathbf{F}_{RL,i} = \frac{\mathbf{F}_{R,i-1/2} - \mathbf{F}_{R,i-3/2}}{2}, \text{ and } \Delta\mathbf{F}_{RR,i} = \frac{\mathbf{F}_{R,i+1/2} - \mathbf{F}_{R,i-1/2}}{2}. \tag{11}$$

The first expression here is the left correction to a right moving wave and the second is the right correction to a right moving wave. Similarly, we can define two second-order flux corrections for left-moving waves:

$$\Delta\mathbf{F}_{LL,i} = -\frac{\mathbf{F}_{L,i+1/2} - \mathbf{F}_{L,i-1/2}}{2}, \text{ and } \Delta\mathbf{F}_{LR,i} = -\frac{\mathbf{F}_{L,i+3/2} - \mathbf{F}_{L,i+1/2}}{2}. \tag{12}$$

There are various formulas, known as limiters, that combine the flux corrections given in Eqs. 11-12 to formulate the final second-order flux corrections. We are only interested in a subset of second-order limiter functions that maintain the TVD property of the algorithm. The simplest TVD limiter is the minmod limiter where the smallest magnitude value is chosen but is zero if the left and right corrections have opposite sign. This can be expressed as

$$\text{minmod: } \phi(a,b) = \frac{1}{2}\left[\text{sign}(a) + \text{sign}(b)\right]\min\left(|a|,|b|\right). \tag{13}$$

The final expressions for the left and right going fluxes given in Eq. 10 are

$$\mathbf{F}_{R,i} = \mathbf{F}^{(0)}_{R,i} + \phi\left(\Delta\mathbf{F}_{RL,i}, \Delta\mathbf{F}_{RR,i}\right), \text{ and } \mathbf{F}_{L,i} = \mathbf{F}^{(0)}_{L,i} + \phi\left(\Delta\mathbf{F}_{LL,i}, \Delta\mathbf{F}_{LR,i}\right), \tag{14}$$

with $\phi(a,b)$ defined in Eq. 13.

4 Sod shock tube problem

The Sod shock tube problem [6] is a Riemann problem for the Euler equations. The Riemann problem is an initial value problem for hyperbolic equations where a piecewise constant initial state has a single discontinuity. The initial state considered by Sod is described by

$$[\rho, u, P] = \begin{cases} [1, 0, 1], & \text{if } x < x_0, \\ [0.125, 0, 0.1], & \text{if } x > x_0. \end{cases} \tag{15}$$

The initial profiles for $x < x_0$ are referred to below as $[\rho_L, u_L, P_L]$ and those for $x > x_0$ are referred to as $[\rho_R, u_R, P_R]$. The adiabatic invariant used for the Sod test is $\gamma = 1.4$. The solution to this problem for $t > 0$ can be obtained analytically. The initial state and the analytic solution at $t = 0.2$ are shown in Fig. 2. The corresponding phase-space diagram of the different characteristics curves that originate from x_0 at $t = 0$ are shown in Fig. 3.

By examining the density profiles in Fig. 2, it is seen that the initial state evolves into five distinct regions. The unperturbed regions far to the left and right of the initial discontinuity are referred to as Region I and Region V, respectively. As the system evolves from its initial state, the high-pressure region flows into the low-pressure region, resulting in a rarefaction wave propagating to the left and a shock wave propagating to the right. In between these regions, there is a contact discontinuity in the density associated with an entropy wave. This position separates the post-shocked gas from Region V, which undergoes an entropy change, from pos-rarefaction gas originating from Region I that has the same entropy as it did initially. Analytic solutions to each of these regions are given in the following subsections.

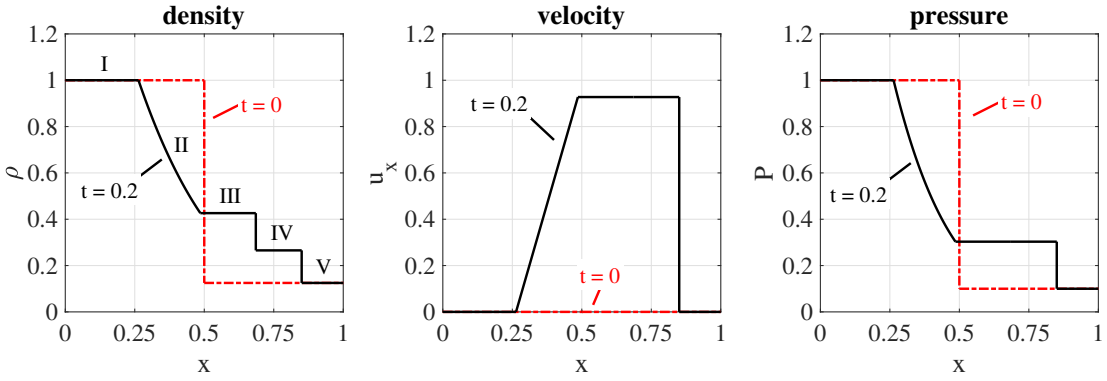

Figure 2: Initial state (dashed red curves) and analytic solution at $t = 0.2$ (solid black curves) for the Sod shock tube problem. The adiabatic coefficient is $\gamma = 1.4$.

4.1 Region II: rarefaction fan

The rarefaction wave in Region II is the only region where the profiles are spatially non-uniform. A rarefaction wave, also known as an expansion wave, is the result of mass leaving a high-pressure region by flowing into a low-pressure region. Rarefaction waves belong to the characteristic family of the Euler equations with the following Riemann invariants: $s, R_{\pm} = u \pm C_s/(\gamma - 1)$, where $s \equiv P/\rho^{\gamma}$ is the specific entropy. These invariants correspond to the eigenvalues $u \pm C_s$ of the flux Jacobian, which are associated with left and right moving waves, respectively. For a left-moving rarefaction wave with homogeneous upstream conditions, the Riemann invariants associated with right-moving characteristics originating upstream of the rarefaction fan (Region I) are constant *everywhere*, and the solution in this region is self-similar such that the slopes of left-going characteristic curves originating inside the expansion fan governed by $dx/dt = u - C_s$ are constant (see Fig. 3 and Appendix B). Thus, the equations governing the fluid quantities in Region II are

$$\frac{P_{\rm II}}{\rho_{\rm II}^{\gamma}} = \frac{P_L}{\rho_L^{\gamma}}, \quad u_{\rm II} + \frac{2C_{\rm II}}{\gamma - 1} = \frac{2C_L}{\gamma - 1}, \quad \frac{x - x_0}{t} = u_{\rm II} - C_{\rm II}. \tag{16}$$

This gives the following explicit formulas for the fluid quantities in Region II:

$$u_{\rm II}(x_1 \le x \le x_2) = \frac{2}{\gamma + 1}\left[\frac{x - x_0}{t} + C_L\right], \tag{17}$$

$$\rho_{\rm II}(x_1 \le x \le x_2) = \left[\frac{\rho_L^{\gamma}}{\gamma P_L}\left[u_{\rm II}(x) - \frac{x - x_0}{t}\right]^2\right]^{\frac{1}{\gamma - 1}}, \tag{18}$$

$$P_{\rm II}(x_1 \le x \le x_2) = \rho_{\rm II}^{\gamma}(x)\frac{P_{\rm L}}{\rho_{\rm L}^{\gamma}}. \tag{19}$$

Setting $u_{\rm II}(x_1) = 0$ in Eq. 17, the leading tip of the rarefaction wave that separates Region I and Region II moves to the left with position given by

$$x_1(t) = x_0 - C_L t. \tag{20}$$

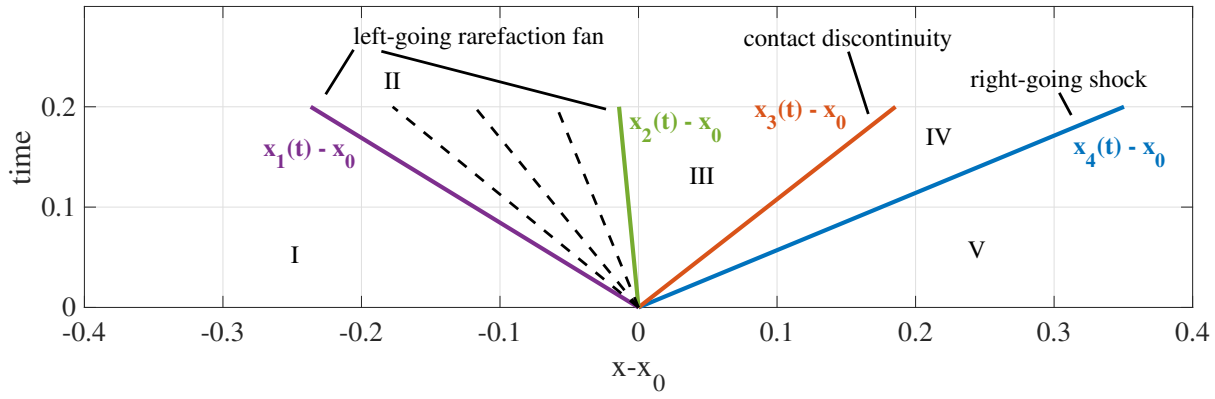

Figure 3: Phase space diagram of characteristic curves for the Sod shock tube problem. Region I is the high-pressure/high-density region to the left of the initial discontinuity. The left-going rarefaction fan is in Region II. Region III is the post rarefaction gas. Region IV is the post-shock gas. Region V is the low-pressure/low-density region to the right of the initial discontinuity.

It is readily seen that the expressions in Eqs. 17-19 agree with the values in Region I for $x = x_1$. The values must match the values in region III at $x = x_2$. This gives the following equation for the position at the right end of the rarefaction wave

$$x_2(t) = x_0 + \left(\frac{\gamma+1}{2} u_{\rm III} - C_L\right) t. \tag{21}$$

$x_1(t)$ and $x_2(t)$ define the boundaries of the rarefaction expansion fan.

A relation that will be used below to close the system is the velocity at x_2 in terms of the pressure. Using Eqs. 17-19 evaluated at x_2 given in Eq. 21, one obtains

$$u_{\rm III} = u_{\rm II}(x_2) = \sqrt{\frac{(1-m^4)\,P_L^{1/\gamma}}{m^4 \rho_L}} \left(P_L^{\frac{\gamma-1}{2\gamma}} - P_{\rm III}^{\frac{\gamma-1}{2\gamma}}\right), \tag{22}$$

where $m^2 \equiv (\gamma-1)/(\gamma+1)$ and we have used $P_{\rm II}(x_2) = P_{\rm III}$.

4.2 Region III: post-rarefaction region

Region III is the post-rarefaction region. This region is separated from the shock region by a contact discontinuity in the density at position x_3, which is also known as an entropy wave. Entropy waves are associated with the eigenvalue $\lambda = u$ and belong to the characteristic family of the Euler equations with the following Riemann invariants: u, P. The velocity and pressure in this region are the same as the post-shock values, but the entropy is different. The entropy is constant at all positions to the left of x_3, which have not experienced the entropy-producing shock. The values in Region III are given by

$$u_{\rm III} = u_{\rm IV}, \quad P_{\rm III} = P_{\rm IV}, \quad \rho_{\rm III} = \rho_L \left(\frac{P_{\rm III}}{P_L}\right)^{1/\gamma}. \tag{23}$$

The position of the contact discontinuity is given by

$$x_3(t) = x_0 + u_{\rm III} t. \tag{24}$$

4.3 Region IV: post-shock region

Region IV is the post-shock region. Shock waves are discontinuous states that occur when a gas moves at a speed greater than the local sound speed. The relationship between the states on either side of a shock is governed by the Rankine-Hugoniot jump conditions, which are derived from the conservation of mass, momentum, and energy in the frame moving with the shock speed u_s. The shock front position and speed are given by

$$x_4(t) = x_0 + u_s t. \tag{25}$$

$$u_s = u_{\rm IV} \frac{\rho_{\rm IV}}{\rho_{\rm IV} - \rho_R}. \tag{26}$$

This relation for u_s comes directly from the conservation of mass in the frame moving with the shock speed and using $u_R = 0$. Post-shock values for the density and velocity can be expressed in terms of the pressure on either side of the shock as

$$\rho_{\rm IV} = \rho_R \frac{P_{\rm IV} + m^2 P_R}{P_R + m^2 P_{\rm IV}}, \tag{27}$$

$$u_{\rm IV} = (P_{\rm IV} - P_R) \sqrt{\frac{1 - m^2}{\rho_R \left(P_{\rm IV} + m^2 P_R\right)}}. \tag{28}$$

The system of equations is closed, and all variables are determined in all regions by solving for the pressure in Region III. This is done by equating the post-shock velocity in Region IV given in Eq. 28 with the velocity at x_2 given by Eq. 22 and using $P_{\rm IV} = P_{\rm III}$, resulting in the following nonlinear equation for $P_{\rm III}$:

$$\sqrt{\frac{\left(1 - m^4\right) P_L^{1/\gamma}}{m^4 \rho_L}} \left(P_L^{\frac{\gamma-1}{2\gamma}} - P_{\rm III}^{\frac{\gamma-1}{2\gamma}} \right) = (P_{\rm III} - P_R) \sqrt{\frac{1 - m^2}{\rho_R \left(P_{\rm III} + m^2 P_R\right)}}. \tag{29}$$

Equation 29 can be solved using a root finding method or a Newton method. For the parameters of the Sod shock tube problem, the solution is $P_{\rm III} = 0.30310$.

5 Simulation Results

Using the algorithm described in Sec. 3, results from numerical simulations of the Sod shock tube problem are presented here. The algorithm is implemented in the COGENT framework [1, 3, 2]. The 1D grid ranges from $x = 0$ to $x = 1$ and N_x below denotes the number of grid points. Simulation results at $t = 0.2$ are shown in Fig. 4 from a low-resolution simulation with $N_x = 100$ and a high-resolution simulation with $N_x = 1600$. The low-resolution simulation results agree qualitatively with the analytic solution. The high-resolution simulation agrees quantitatively with the analytic solution.

The shock front separating regions IV and V is the most challenging one to resolve in the sod shock tube problem. Fig. 5 shows convergence of the numerical solution near the shock front to the analytic solution with increasing grid resolution.

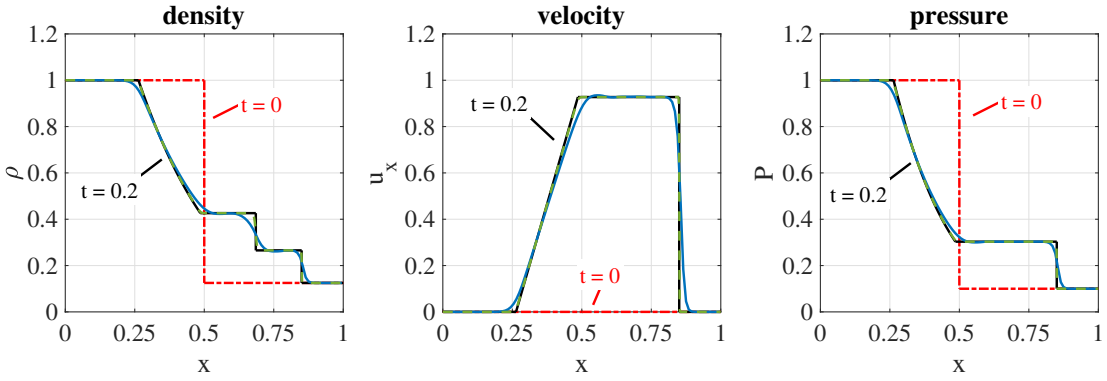

Figure 4: Numerical simulation results of the Sod shock tube problem at $t = 0.2$. The solid blue curves are results from low-resolution ($N_x = 100$) simulations. The dashed green curves are results from high-resolution ($N_x = 1600$) simulations. The initial state is shown by the dashed red curves and the analytic solution at $t = 0.2$ is shown by the solid black curves.

A Euler Equations in Two Dimensions

The Euler equations in 2D are

$$\frac{\partial \mathbf{w}}{\partial t} + \frac{\partial \mathbf{F}(\mathbf{w})}{\partial x} + \frac{\partial \mathbf{G}(\mathbf{w})}{\partial y} = 0. \tag{30}$$

where

$$\mathbf{w} = \begin{bmatrix} \rho \\ \rho u_x \\ \rho u_y \\ \mathcal{E} \end{bmatrix}, \quad \mathbf{F}(\mathbf{w}) = \begin{bmatrix} \rho u_x \\ \rho u_x^2 + P \\ \rho u_y u_x \\ (\mathcal{E} + P)\, u_x \end{bmatrix}, \quad \mathbf{G}(\mathbf{w}) = \begin{bmatrix} \rho u_y \\ \rho u_x u_y \\ \rho u_y^2 + P \\ (\mathcal{E} + P)\, u_y \end{bmatrix}. \tag{31}$$

The eigenvalues of the flux Jacobian $\partial \mathbf{F}/\partial \mathbf{w}$ are $\lambda = [u_x \pm C_s, u_x, u_x]$. The eigenvalues of the flux Jacobian $\partial \mathbf{G}/\partial \mathbf{w}$ are $\lambda = [u_y \pm C_s, u_y, u_y]$. A commonly used flux freezing speed, which is computed locally on the grid, for Lax flux splitting is $|\mathbf{u}| + C_s$ [4, 7].

B Riemann Invariants for 1D Isentropic Flow

To better explain the solution in Region II, consider a 1D isentropic flow where the specific entropy $s = P/\rho^\gamma$ is constant. The 1D Euler equations reduce to a two-variable system and can be written in non-conservative form as

$$\begin{bmatrix} \rho \\ u \end{bmatrix}_t + \begin{bmatrix} u & \rho \\ \frac{c_s^2}{\rho} & u \end{bmatrix} \begin{bmatrix} \rho \\ u \end{bmatrix}_x = \begin{bmatrix} 0 \\ 0 \end{bmatrix}. \tag{32}$$

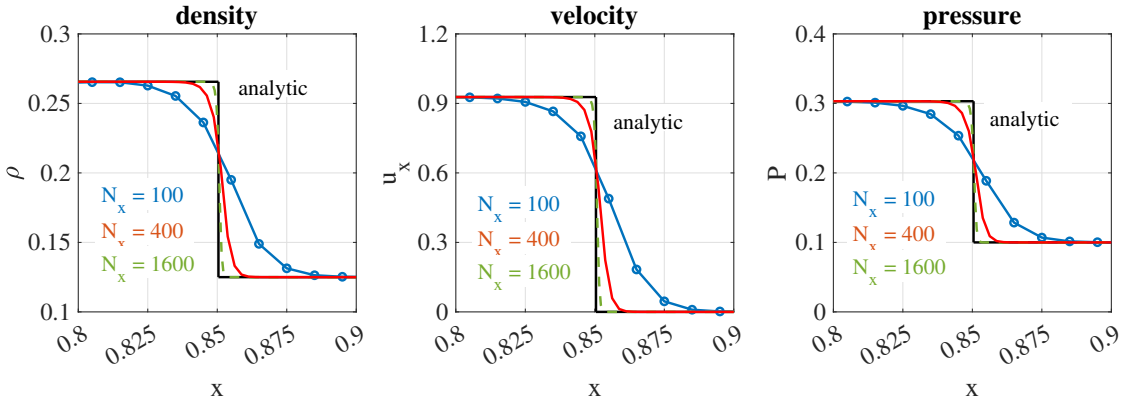

Figure 5: Shock front resolution scan with grid spacing Δx for the Sod shock tube problem.

The eigenvalues of this flux Jacobian are $\lambda = u \pm C_s$. The left eigenvectors are $\mathbf{L}_\pm = [\pm C_s/\rho, 1]$. The Riemann invariants are given by

$$\mathbf{L}_\pm \cdot d\mathbf{w} = 0 \quad \Rightarrow \quad R_\pm = u \pm \int \frac{C_s}{\rho} d\rho = u \pm \frac{2C_s}{\gamma - 1} = \text{constant along } \frac{dx}{dt} = u \pm C_s. \tag{33}$$

With some effort, the original system given in Eq. 32 can be re-written as

$$\frac{\partial R_\pm}{\partial t} + (u \pm C_s) \frac{\partial R_\pm}{\partial x} = 0. \tag{34}$$

Strictly speaking, $R_\pm$ are constant along characteristic curves with trajectories given by $dx/dt = u_x \pm C_s$. However, since all right-going characteristics inside the expansion fan for the Sod shock tube problem originate from the same uniform state on the left side of the initial discontinuity, R_+ is constant *everywhere*, not just along the associated characteristic curve, and the equation for R_+ is trivially satisfied. In this case, the equation for R_- has self-similar solutions of the form $R_-(x,t) = R_-\left(x/t = u - C_s\right)$, which means that the associated characteristic curves have a constant slope.

Acknowledgments

This work was performed under the auspices of the U.S. Department of Energy by Lawrence Livermore National Laboratory under Contract DE-AC52-07NA27344 and was supported by DARPA's NaPSAC Program. LLNL-TR-2002288.

References

[1] J. R. Angus, M. Dorf, and V. I. Geyko. Drift-ideal magnetohydrodynamic simulations of mâ=â0 modes in z-pinch plasmas. *Physics of Plasmas*, 26(7):072505, 2019.

[2] Mikhail Dorf and Milo Dorr. Continuum kinetic modelling of cross-separatrix plasma transport in a tokamak edge including self-consistent electric fields. *Contributions to Plasma Physics*, 58(6-8):434–444, 2018.

[3] Milo R. Dorr, Phillip Colella, Mikhail A. Dorf, Debojyoti Ghosh, Jeffrey A.F. Hittinger, and Peter O. Schwartz. High-order discretization of a gyrokinetic vlasov model in edge plasma geometry. *Journal of Computational Physics*, 373:605 – 630, 2018.

[4] Shi Jin and Zhouping Xin. The relaxation schemes for systems of conservation laws in arbitrary space dimensions. *Communications on Pure and Applied Mathematics*, 48(3):235–276, 1995.

[5] Shahram Karami, Paul C. Stegeman, Andrew Ooi, and Julio Soria. High-order accurate large-eddy simulations of compressible viscous flow in cylindrical coordinates. *Computers and Fluids*, 191:104241, 2019.

[6] Gary A Sod. A survey of several finite difference methods for systems of nonlinear hyperbolic conservation laws. *Journal of Computational Physics*, 27(1):1 – 31, 1978.

[7] Hy Trac and Ue-Li Pen. A primer on eulerian computational fluid dynamics for astrophysics. *Publications of the Astronomical Society of the Pacific*, 115(805):303, 2003.

[8] Xiangxiong Zhang and Chi-Wang Shu. Positivity-preserving high order finite difference weno schemes for compressible euler equations. *Journal of Computational Physics*, 231(5):2245 – 2258, 2012.